Hyperfine structure in the atomic spectrum of niobium

I: Experimental investigation

A. Bouzed[1], S. Kröger[2,a], D. Zimmermann[2], H.-D. Kronfeldt[1], and G. Guthöhrlein[3]

[1] Optisches Institut, Technische Universität Berlin, Hardenbergstr. 36, 10623 Berlin, Germany
[2] Institut für Atomare Physik und Fachdidaktik, Technische Universität Berlin, Hardenbergstr. 36, 10623 Berlin, Germany
[3] Laboratorium für Experimentalphysik, Universität der Bundeswehr Hamburg, Holstenhofweg 85, 22043 Hamburg, Germany

Abstract. We report on hyperfine structure measurements in 21 lines of atomic niobium in the spectral region from 640 nm to 870 nm by means of optogalvanic laser spectroscopy and laser induced fluorescence spectroscopy using a hollow cathode discharge and a tunable single-mode cw ring laser. Hyperfine structure constants A and B of altogether 29 excited energy levels were determined, 18 of them for the first time.

PACS. 32.30.Jc Visible and ultraviolet spectra – 31.30.Gs Hyperfine interactions and isotope effects, Jahn-Teller effect

1 Introduction

The atomic spectrum of niobium is characterized by the large hyperfine structure of the only stable isotope ^{93}Nb with nuclear spin 9/2 caused by the large nuclear magnetic dipole moment of $\mu_I = 6.1705\,(3)\,\mu_N$ [1]. Therefore in many transitions it is adequate to apply Doppler limited experimental techniques for an accurate determination of the hyperfine interaction constants A. In contrast to the large magnetic dipole interaction the additional shift caused by the electric quadrupole interaction is very small due to the small nuclear electric quadrupole moment $Q = -0.36\,(7)$ b [1]. For this reason it is difficult to get precise values of the B constants from optical spectroscopy.

Up to now, the hyperfine structure of 52 levels of Nb I has been determined using different experimental methods. The two lowest multiplets $4d^4 5s$ ^{6}D and $4d^3 5s^2$ ^{4}F have been studied with high accuracy by Büttgenbach *et al.* [2] using the atomic beam magnetic resonance method. Fraenkel *et al.* [3] reported on the hfs interaction constants of 17 metastable levels of the three even configurations $4d^3 5s^2$, $4d^4 5s$ and $4d^5$ and 14 levels of the odd configurations $4d^3 5s 5p$ and $4d^4 5p$ by means of high resolution laser and radio frequency double resonance techniques. In the wavelength region covered by the dye rhodamine 6G Doppler limited optogalvanic laser spectroscopy technique was applied by Singh *et al.* [4,5] to study the hy-

perfine structure of altogether 34 excited levels. Using resonance ionization spectroscopy the hyperfine splitting of the ground level and of three odd and one even excited level were measured by Lauranto *et al.* [6].

In the present work we report on an experimental determination of the hyperfine structure constants of levels of the even configurations $4d^3 5s^2$, $4d^4 5s$, $4d^5$, $4d^4 6s$ and $4d^3 5s 6s$ and the odd configurations $4d^4 5p$ and $4d^3 5s 5p$ using optogalvanic laser spectroscopy and laser induced fluorescence spectroscopy. A detailed parametric hyperfine structure analysis based on these data is given in a separate paper [7].

2 Experimental

Doppler-limited optogalvanic laser spectroscopy and laser induced fluorescence spectroscopy with a tunable single-mode cw ring laser (titanium-sapphire or dye laser with DCM) was applied to investigate the hyperfine structure. A see-through hollow cathode lamp with a liquid nitrogen cooling system [8] served to evaporate the niobium. The cathode was 15 mm long and had a 3 mm bore whose surface was covered with a 0.125 mm Nb foil. The hollow cathode gas discharge was run with a current between 40 mA and 70 mA in an argon atmosphere at around 1 mbar. More details of the experimental setup are given in [9].

Altogether 21 lines of atomic Nb have been investigated in the spectral range from 640 nm to 870 nm.

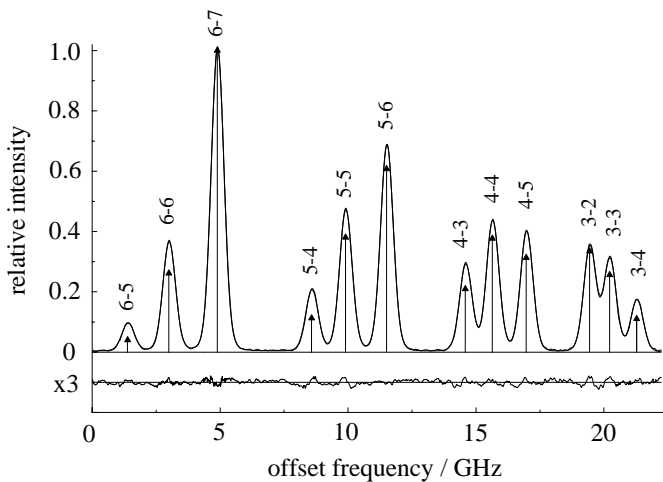[a] e-mail: `sk@kalium.physik.tu-berlin.de`

Energy level scheme (Fig. 1):

even parity (upper):
39100.73 — 4d³5s6s
38638.47 — 4d³5s6s
38567.85 — 4d⁴6s
38276.59 — 4d³5s6s
38177.65 — 4d⁴6s
38021.41 — 4d³5s6s   even
37871.30 — 4d³5s6s
37842.36 — 4d⁴6s
37578.72 — 4d⁴6s
37410.17 — 4d⁴6s

upper transition wavelengths: 867.04, 855.85, 854.54, 851.89, 851.75, 849.00, 846.79, 833.70, 824.34, 823.39, 818.81

odd parity (middle):
28535.36 — 4d³5s5p
27419.62 — 4d³5s5p
26832.43 — 4d³5s5p
26440.33 — 4d⁴5p
26067.06 — 4d³5s5p
26060.65 — 4d⁴5p
25930.01 — 4d⁴5p   odd
25879.81 — 4d³5s5p
24773.03 — 4d⁴5p
24506.53 — 4d³5s5p
24396.80 — 4d⁴5p
23574.14 — 4d³5s5p
21512.18 — 4d³5s5p

lower transition wavelengths: 853.10, 843.70, 832.09, 816.06, 672.36, 670.99, 666.08, 660.73, 654.46, 643.05

even parity (lower):
14211.30 — 4d⁴5s
13629.15 — 4d⁴5s
13404.77 — 4d³5s²
9497.52 — 4d⁴5s   even
8705.32 — 4d⁴5s
5965.45 — 4d³5s²

Fig. 1. Part of the energy level scheme of Nb I showing the transitions investigated; energies are in cm^{-1} (not to scale), wavelengths are in nm. Electronic configuration and parity are given at the right.

They are summarized in Figure 1 showing part of the energy level scheme of Nb I. The lines measured by means of optogalvanic spectroscopy are listed in Table 1 and those measured by means of laser induced fluorescence spectroscopy in Table 2 with the specification of the fluorescence wavelength. In some cases the lines lie very close, so that the hyperfine spectra of two neighbouring lines are overlapping. To separate such lines the method of laser induced fluorescence is required.

All six lines of Table 1 and one of the 15 lines of Table 2 are already listed in the M.I.T. wavelength tables [10]. The remaining 14 lines (given without an intensity entry in Tab. 2) are new lines. Their wavelengths have been calculated from the energy difference of selected known levels, one of them being of particular interest in every case. By finding consistent niobium hyperfine patterns using the expected wavelengths λ_f for the laser induced fluorescence detection we feel ultimate confidence in these new lines.

An example of a 12 component hyperfine pattern measured by applying laser induced fluorescence spectroscopy is presented in Figure 2 together with the best fit.

Table 1. Nb I transitions investigated by means of optogalvanic spectroscopy; wavelengths and intensities are according to [10]; *italic*: levels of odd parity.

		lower level		upper level	
λ_air/nm	int.	E/cm^{-1}	J	E/cm^{-1}	J
643.046	80	5 965.45	5/2	*21 512.18*	*7/2*
654.461	80	9 497.52	7/2	*24 773.03*	*5/2*
660.7276	15	13 404.77	5/2	*28 535.36*	*7/2*
666.084	300	9 497.52	7/2	*24 506.53*	*9/2*
670.988	15	9 497.52	7/2	*24 396.80*	*5/2*
672.362	100	8 705.32	3/2	*23 574.14*	*5/2*

Table 2. Nb I transitions investigated by means of laser induced fluorescence spectroscopy with specification of the fluorescence wavelength λ_f ($^+$: decay of the upper level of the laser transition, $^-$: decay of the lower level); intensities according to [10]; *italic*: levels of odd parity.

		lower level		upper level		
λ_air/nm	int.	E/cm^{-1}	J	E/cm^{-1}	J	λ_f/nm
816.058		13 629.15	1/2	*25 879.81*	*1/2*	388.61$^+$
818.807		*26 067.06*	*3/2*	38 276.59	5/2	389.37$^-$
823.388		*25 879.81*	*1/2*	38 021.41	3/2	388.61$^-$
824.344		*26 440.33*	*9/2*	38 567.85	9/2	590.06$^-$
832.093	500	9 497.52	7/2	*21 512.18*	*7/2*	534.42$^-$
833.695		*25 879.81*	*1/2*	37 871.30	1/2	388.61$^-$
843.696		14 211.30	3/2	*26 060.65*	*5/2*	576.03$^+$
846.790		*26 832.43*	*7/2*	38 638.47	7/2	387.76$^-$
849.001		*26 067.06*	*3/2*	37 842.36	5/2	389.37$^-$
851.748		*26 440.33*	*9/2*	38 177.65	7/2	590.06$^-$
851.887		*26 832.43*	*7/2*	38 567.85	9/2	387.76$^-$
853.101		14 211.30	3/2	*25 930.01*	*3/2*	570.65$^+$
854.541		*25 879.81*	*1/2*	37 578.72	3/2	388.61$^-$
855.850		*27 419.62*	*9/2*	39 100.73	9/2	379.21$^-$
867.037		*25 879.81*	*1/2*	37 410.17	1/2	388.61$^-$

In order to obtain the hyperfine interaction constants A and B the recorded spectra have been fitted using Voigt profiles for the individual hyperfine components. The fit parameters were the centre of gravity of the total hyperfine structure, the A and B constants of the upper and the lower level, the Gaussian and Lorentzian part of the Voigt profile and two parameters to take into account background and slope. Depending on the discharge current the Gaussian line width varied from 800 MHz to 1000 MHz for the lines in the red wavelength region and from 550 MHz

Fig. 2. Experimental intensity distribution of the Nb I transition $4d^4 5s$ $^4\mathrm{P}_{3/2}$ $\longrightarrow$ $4d^4 5p$ $^4\mathrm{F}_{5/2}$ at $\lambda = 843.696$ nm measured with laser induced fluorescence spectroscopy together with the best fitted curve. In the lower part of the figure the residuals between experiment and calculation are given, multiplied with a factor of 3. The components are assigned by the total angular momentum F of the lower and upper hyperfine levels. The theoretical intensities are indicated by arrows relative to the intensity of the strongest component.

to 700 MHz for the lines in the near infrared region, corresponding to a Boltzmann temperature of about 500 to 800 K.

In most cases the observed intensity ratios of the hyperfine structure components differ from the theoretical intensity ratios. This is caused by two different effects, namely hyperfine pumping and a saturation for high laser intensity. The latter effect results in an intensity reduction and broadening of the strong hyperfine components, which leads to an apparent intensity increase of the weak components. As a consequence the Lorentzian contribution differs for the individual hyperfine components and the ratio of the intensities of the components is not in accordance with the theoretical ratios calculated for local thermodynamic equilibrium. For this reason all spectra with well separated hyperfine components are fitted with individual profile parameters and intensity parameters for each hyperfine component. To show the intensity increase of the weak components in Figure 2 the theoretical relative intensities are given as arrows (the arrows are normalized to the strongest hyperfine component).

To analyze the spectra showing unresolved hyperfine structure the number of parameters had to be reduced. For this reason the ratio of the Lorentzian line width and the intensities of the different components were fixed to the ratios obtained from a fit of another spectrum with the same J quantum numbers and well separated hyperfine components whereas the Gaussian line widths of all components were assumed to be equal. Sometimes the values of the hyperfine constants A and B of one level have been fixed additionally if they were already known from literature. These hyperfine constants are marked in Table 3 with an asterisk.

3 Results

The magnetic dipole and electric quadrupole hyperfine interaction constants A and B of altogether 29 energy levels have been determined experimentally. Out of these, the values of nine (from 16) even parity levels and also of nine (from 13) odd parity levels have been measured for the first time. In Table 3 the results are compiled together with all A and B values found in the literature for the even parity levels and equally in Table 4 for the odd parity levels. The hyperfine spectrum of each of the investigated lines has been recorded and fitted ten times. The given A and B constants are the mean of the "Best"-values of the ten fits, the error margins are the standard deviation. In the cases, where the hyperfine interaction constants of one of the combining levels were fixed during the fit, the errors given take into account the standard deviation and the error propagation due to the error margins of the introduced hyperfine interaction constants.

With few exceptions, the A and B values from different sources agree within the limits of error.

One exception is the level $4d^4 5s$ $b^4\mathrm{P}_{3/2}$ at $14\,211.30$ cm^{-1}, where our results show a very large deviation from the values given in [5]. To check our results, we have determined the A and B constants of this level by evaluating the hyperfine spectra of two spectral lines starting from this level. The good consistence of the obtained results is obvious (see Tab. 3).

The other exception refers to the levels $18\,791.09$ cm^{-1} and $25\,879.81$ cm^{-1} (see Tab. 4). These are levels where energy differences measured by resonance ionization spectroscopy from [6] were used for the determination of the A values. The inconsistency is not only between our values and those from [6] but also between values from [4] and [6]. One of our values was confirmed by investigation of different transitions. We could not find any reason for this huge discrepancy. Three of the five values determined from [6] are in agreement with the values of other authors.

4 Conclusion

Optogalvanic and laser induced fluorescence spectroscopy in a hollow cathode discharge were performed for the determination of the magnetic dipole hyperfine structure constants A of Nb I with high accuracy. The measured electric quadrupole hyperfine structure constants B are less accurate, due to the very small nuclear electric quadrupole moment. However, the accuracy of the B constants is comparable with the accuracy of other optical measurements [4,5].

Hyperfine structure data of altogether 29 excited energy levels have been achieved, greatly extending previous data. The large quantity of new hyperfine structure data together with the data available from the literature provides an enlarged basis suitable for a detailed theoretical analysis using the effective operator formalism. This will be treated in part II of this work [7] for the even configurations.

Table 3. Experimental hyperfine structure constants A and B of the levels of even parity of Nb I from the present work and from [2–6]. The wavelength given in column 3 specifies the line which was used to determine the A and B values, m: determined from more than one transition; abmr: atomic beam magnetic resonance technique, ris: resonance ionization spectroscopy, lrf: laser radiofrequency double resonance technique, ogs: optogalvanic spectroscopy, lif: laser induced spectroscopy.

E/cm^{-1}	level	$\lambda_{\mathrm{air}}/\mathrm{nm}$	A/MHz	B/MHz	method	references
0.00	$4d^4 5s$ $^6\mathrm{D}_{1/2}$		1 868.2184 (18)	0	abmr	[2]
			1 840†	0	ris	[6]
154.19	$4d^4 5s$ $^6\mathrm{D}_{3/2}$		852.5428 (21)	−64.572 (41)	abmr	[2]
391.99	$4d^4 5s$ $^6\mathrm{D}_{5/2}$		719.4759 (18)	−47.605 (39)	abmr	[2]
695.25	$4d^4 5s$ $^6\mathrm{D}_{7/2}$		690.1978 (16)	20.475 (75)	abmr	[2]
1 050.26	$4d^4 5s$ $^6\mathrm{D}_{9/2}$		691.6141 (22)	132.754 (116)	abmr	[2]
1 142.79	$4d^3 5s^2$ $^4\mathrm{F}_{3/2}$		644.16 (54)	32.800 (128)	abmr	[2]
		566.470	634.7 (10.0)	30.8 (30.0)	ogs	[4]
1 586.90	$4d^3 5s^2$ $^4\mathrm{F}_{5/2}$		372.4853 (17)	33.341 (38)	abmr	[2]
2 154.11	$4d^3 5s^2$ $^4\mathrm{F}_{7/2}$		292.2022 (16)	44.928 (47)	abmr	[2]
		578.751	289.5 (10.0)	65.3 (30.0)	ogs	[4]
2 805.36	$4d^3 5s^2$ $^4\mathrm{F}_{9/2}$		269.6320 (26)	64.315 (130)	abmr	[2]
		584.246	279.4 (10.0)	64.7 (30.0)	ogs	[4]
4 998.17	$4d^3 5s^2$ $^4\mathrm{P}_{1/2}$	587.776	540.1 (0.9)	0	lrf	[3]
		587.776	537.4 (6.0)	0	ogs	[5]
5 297.92	$4d^3 5s^2$ $^4\mathrm{P}_{3/2}$	598.322	497.7569 (16)	59.902 (14)	lrf	[3]
		598.322	495.5 (6.0)	30 (35)	ogs	[5]
5 965.45	$4d^3 5s^2$ $^4\mathrm{P}_{5/2}$	586.643	343.1670 (5)	−80.454 (9)	lrf	[3]
		586.643	341.3 (10.0)	−122.2 (30.0)	ogs	[5]
		643.046	343.4 (1.1)	−76 (5)	ogs	this work
8 410.90	$4d^4 5s$ $^4\mathrm{D}_{1/2}$	570.647	1 997.0 (1.1)	0	lrf	[3]
		570.647	2 001.7 (10.0)	0	ogs	[5]
8 705.32	$4d^4 5s$ $^4\mathrm{D}_{3/2}$	580.401	−143.3225 (217)	−10.761 (178)	lrf	[3]
		576.032	−136.9 (6.0)	−69 (35)	ogs	[5]
		672.362	−142.7 (1.6)	7 (17)	ogs	this work
8 827.00	$4d^3 5s^2$ $^2\mathrm{G}_{7/2}$	580.099	420.2938 (11)	−49.006 (36)	lrf	[3]
9 043.14	$4d^4 5s$ $^4\mathrm{D}_{5/2}$	587.467	−407.8606 (43)	35.060 (75)	lrf	[3]
		583.860	−408.6 (10.0)	38.9 (30.0)	ogs	[4]
9 328.88	$4d^3 5s^2$ $^2\mathrm{G}_{9/2}$	584.242	358.5642 (8)	−61.048 (30)	lrf	[3]
9 439.08	$4d^3 5s^2$ $^2\mathrm{D}_{3/2}$	584.178	389.1039 (23)	73.590 (19)	lrf	[3]
9 497.52	$4d^4 5s$ $^4\mathrm{D}_{7/2}$	591.943	−477.0373 (35)	126.899 (81)	lrf	[3]
		590.057	−474.4 (2.0)	90 (35)	ogs	[5]
		654.461	−477.3 (1.8)	88 (50)	ogs	this work
		670.988	−478.0 (1.7)	98 (30)	ogs	this work
		832.093	−476.9 (6)	131 (8)	lif	this work
		666.084	−475 (2)	86 (50)	ogs	this work
10 126.06	$4d^3 5s^2$ $^2\mathrm{P}_{1/2}$	602.545	323.6590 (4)	0	lrf	[3]
10 237.51	$4d^3 5s^2$ $^2\mathrm{D}_{5/2}$	m	295.6803 (6)	36.501 (12)	lrf	[3]
11 318.09	$4d^3 5s^2$ $^2\mathrm{P}_{3/2}$	583.811	167.3182 (25)	−5.805 (21)	lrf	[3]
11 344.70	$4d^5$ $^6\mathrm{S}_{5/2}$	590.380	−639.3786 (79)	−0.061 (92)	lrf	[3]
		m	−644.5 (6.5)	–	ogs	[5]
12 018.25	$4d^4 5s$ $^2\mathrm{G}_{5/2}$	581.533	−101.2 (6.0)	–	ogs	[5]
12 102.12	$4d^3 5s^2$ $^2\mathrm{H}_{9/2}$	582.254	384.9669 (33)	−163.323 (96)	lrf	[3]
13 404.77	$4d^3 5s^2$ $^4\mathrm{F}_{5/2}$	577.483	302.525555 (9)	−43.908 (19)	lrf	[3]
		660.730	305 (4)	−24 (20)	ogs	this work
13 515.20	$4d^3 5s^2$ $^4\mathrm{F}_{7/2}$	581.190	136.9050 (6)	−48.916 (14)	lrf	[3]
13 629.15	$4d^4 5s$ $^4\mathrm{P}_{1/2}$	569.788	2 906.3 (6.0)	0	ogs	[5]
		816.058	2 939.1 (8)	0	lif	this work

Table 3. *Continued.*

E/cm^{-1}	level		$\lambda_{\text{air}}/\text{nm}$	A/MHz	B/MHz	method	references
14 211.30	$4d^45s$	$^4\text{P}_{3/2}$	589.343	−787.0 (6.0)	−100 (35)	ogs	[5]
			843.696	1 414.5 (2)	31 (4)	lif	this work
			853.101	1 414.4 (4)	29 (3)	lif	this work
15 282.35	$4d^45s$	$^4\text{D}_{7/2}$	m	957.3 (5.0)	–	ogs	[5]
18 035.97	$4d^45s$	$^2\text{G}_{9/2}$	m	707.8 (6.0)	18.0 (35.0)	ogs	[5]
37 410.17	$4d^46s$	$^6\text{D}_{1/2}$	867.037	−986.3 (4)	0	lif	this work
37 578.72	$4d^46s$	$^6\text{D}_{3/2}$	854.541	−199.0 (2)	−70 (6)	lif	this work
37 842.36	$4d^46s$	$^6\text{D}_{5/2}$	849.001	−86.4 (1.8)*	−47 (30)*	lif	this work
37 871.30	$4d^35s6s$	$^6\text{F}_{1/2}$		1 800†	0	ris	[6]
			833.695	−1 749.9 (5)	0	lif	this work
38 021.41	$4d^35s6s$	$^6\text{F}_{3/2}$	823.388	547.7 (6)	−24 (5)	lif	this work
38 177.65	$4d^46s$	$^6\text{D}_{7/2}$	851.748	−37 (3)	42 (13)	lif	this work
38 276.59	$4d^35s6s$	$^6\text{F}_{5/2}$	818.807	871.9 (1.0)	−10 (14)	lif	this work
38 567.85	$4d^46s$	$^6\text{D}_{9/2}$	851.887	4.4 (7)	112 (50)	lif	this work
			824.344	5 (2)*	126 (8)*	lif	this work
38 638.47	$4d^35s6s$	$^6\text{F}_{7/2}$	846.790	958.5 (8)	−59 (17)	lif	this work
39 100.73	$4d^35s6s$	$^6\text{F}_{9/2}$	855.850	981.8 (7)	67 (30)	lif	this work

*: A and B constants of the lower level fixed during the fit.
†: A calculated from the energy difference of the hyperfine levels.

Table 4. Experimental hyperfine structure constants A and B of the levels of odd parity of Nb I from the present work and from [2–6]. The wavelength given in column 3 specifies the line which was used to determine the A and B values, m: determined from more than one transition; ris: resonance ionization spectroscopy, lrf: laser radiofrequency double resonance technique, ogs: optogalvanic spectroscopy, lif: laser induced spectroscopy.

E/cm^{-1}	level		$\lambda_{\text{air}}/\text{nm}$	A/MHz	B/MHz	method	references
18 791.09	$4d^35s5p$	$^6\text{F}_{1/2}$		1 760†	0	ris	[6]
			566.470	−779.6 (10.0)	0	ogs	[4]
19 427.90	$4d^35s5p$	$^6\text{F}_{5/2}$	578.751	654.7 (10.0)	7.0 (30.0)	ogs	[4]
19 916.69	$4d^35s5p$	$^6\text{F}_{7/2}$	584.246	680.6 (10.0)	−277.7 (30.0)	ogs	[4]
21 512.18	$4d^35s5p$	$^4\text{D}_{7/2}$	832.093	872.0 (7)	−34 (5)	lif	this work
			643.046	873.2 (5)	−41 (40)	ogs	this work
22 006.74	$4d^45p$	$^4\text{P}_{1/2}$	m	−267.3 (3)	0	lrf	[3]
			m	−272.3 (1.3)	0	ogs	[5]
23 006.86	$4d^45p$	$^4\text{P}_{3/2}$	586.643	−137.9 (4)	−30.9 (3.7)	lrf	[3]
			586.643	−145.1 (10.0)	−17.3 (30.0)	ogs	[4]
23 574.14	$4d^35s5p$	$^4\text{F}_{5/2}$	672.362	514.5 (9)	94 (30)	ogs	this work
24 396.80	$4d^45p$	$^6\text{F}_{5/2}$	670.988	277 (3)	−45 (30)	ogs	this work
24 506.53	$4d^35s5p$	$^4\text{F}_{9/2}$	666.084	594 (3)	70 (50)	ogs	this work
24 773.03	$4d^45p$	$^2\text{D}_{5/2}$	654.461	170.2 (1.9)	−24 (30)	ogs	this work
25 879.81	$4d^35s5p$	$^6\text{D}_{1/2}$		4 400†	0	ris	[6]
			823.388	1 537.4 (1.0)	0	lif	this work
			833.695	1 537.7 (9)	0	lif	this work
			816.058	1 538.3 (8)	0	lif	this work
			867.037	1 538.1 (1.2)	0	lif	this work
			854.541	1 538.2 (9)	0	lif	this work
25 930.01	$4d^45p$	$^4\text{F}_{3/2}$	m	557.4 (5)	57.5 (4.0)	lrf	[3]
			570.647	559.6 (10.0)	100.5 (30.0)	ogs	[4]
			853.101	557.2 (3.0)	58 (3)	lif	this work

Table 4. *Continued.*

E/cm^{-1}	level		$\lambda_{\mathrm{air}}/\mathrm{nm}$	A/MHz	B/MHz	method	references
26 060.65	$4d^45p$	$^4\mathrm{F}_{5/2}$	m	266.7 (3)	46.1 (4.8)	lrf	[3]
			576.032	261.1 (3.0)	–	ogs	[5]
			843.696	266.7 (2)	45 (5)	lif	this work
26 067.06	$4d^35s5p$	$^6\mathrm{D}_{3/2}$	818.807	943.5 (1.8)	79 (3)	lif	this work
26 165.79	$4d^45p$	$^4\mathrm{F}_{7/2}$	583.860	299.6 (10.0)	96.4 (30.0)	ogs	[4]
26 386.36	$4d^35s5p$	$^6\mathrm{D}_{5/2}$	591.943	809.2 (5)	64.2 (9.3)	lrf	[3]
26 440.33	$4d^45p$	$^4\mathrm{F}_{9/2}$	584.242	337.6 (2)	88.6 (8.1)	lrf	[3]
			590.057	325.0 (2.0)	–	ogs	[5]
			851.748	337 (2)	49 (8)	lif	this work
26 552.40	$4d^45p$	$^6\mathrm{D}_{1/2}$	584.178	430.1 (5)	0	lrf	[3]
26 713.32	$4d^45p$	$^6\mathrm{D}_{3/2}$	606.782	108.6 (4)	−19.6 (3.0)	lrf	[3]
26 717.73	$4d^45p$	$^4\mathrm{D}_{1/2}$	602.545	508.3 (4)	0	lrf	[3]
				$480^\dagger$	0	ris	[6]
26 832.43	$4d^35s5p$	$^6\mathrm{D}_{7/2}$	846.790	379.0 (8)	−95 (20)	lif	this work
			851.887	377.4 (1.0)	−105 (20)	lif	this work
27 419.62	$4d^35s5p$	$^6\mathrm{D}_{9/2}$	855.850	405.4 (9)	94 (20)	lif	this work
27 427.07	$4d^45p$	$^6\mathrm{D}_{7/2}$	581.587	386.0 (5)	−382. (15.2)	lrf	[3]
28 278.25	$4d^35s5p$	$^6\mathrm{P}_{3/2}$	590.380	747.1 (8)	14.7 (7.6)	lrf	[3]
			590.380	743.2 (6.0)	19.0 (35.0)	ogs	[5]
28 442.16	$4d^35s5p$	$^2\mathrm{P}_{1/2}$	583.811	2 242.7 (1.2)	0	lrf	[3]
28 445.33	$4d^35s5p$	$^4\mathrm{P}_{5/2}$	584.612	607.8 (6.0)	150.0 (35.0)	ogs	[5]
28 535.36	$4d^35s5p$	$^4\mathrm{F}_{7/2}$	660.730	662 (3)	27 (40)	ogs	this work
28 652.66	$4d^35s5p$	$^6\mathrm{P}_{5/2}$	577.608	746.2 (6.0)	−154.0 (35.0)	ogs	[5]
29 209.42	$4d^35s5p$	$^4\mathrm{D}_{7/2}$	581.533	505.4 (6.0)	–	ogs	[5]
29 271.99	$4d^35s5p$	$^4\mathrm{H}_{7/2}$	582.254	−189.5 (3)	−10.6 (8.2)	lrf	[3]
30 716.50	$4d^45p$	$^4\mathrm{F}_{5/2}$	m	477.8 (4)	45.8 (7.2)	lrf	[3]
31 174.65	$4d^35s5p$	$^4\mathrm{S}_{3/2}$	m	1 047.0 (6.0)	8.8 (35.0)	ogs	[5]
32 605.39	$4d^45p$	$^4\mathrm{F}_{9/2}$	577.106	264.7 (4.0)	–	ogs	[5]
32 802.44	$4d^45p$	$^4\mathrm{G}_{9/2}$	570.615	632.5 (3.0)	16.5 (35.0)	ogs	[5]
35 156.94	$4d^45p$	$^4\mathrm{G}_{9/2}$	583.917	632.5 (6.0)	–	ogs	[5]
35 496.39	$4d^45p$	$^2\mathrm{H}_{9/2}$	572.565	522.7 (6.0)	−58.0 (35.0)	ogs	[5]

$\dagger$: A calculated from the energy difference of the hyperfine levels.

References

1. C.M. Lederer, V.S. Shirley, *Tables of Isotopes*, 7th edn. (Wiley, New York, 1978)
2. S. Büttgenbach, R. Dicke, H. Gebauer, M. Herschel, G. Meisel, Z. Phys. A **275**, 193 (1975)
3. L. Fraenkel, C. Bengtsson, D. Hanstrop, A. Nyberg, J. Persson, Z. Phys. D **8**, 171 (1988)
4. R. Singh, G.N. Rao, Phys. Scripta **40**, 170 (1989)
5. R. Singh, R.K. Thareja, G.N. Rao, J. Opt. Soc. Am. B **9**, 493 (1992)
6. H.M. Lauranto, I.H. Auterinen, T.T. Kajava, K.M. Nyholm, R.R.E. Salomaa, Appl. Phys. B **50**, 323 (1990)
7. S. Kröger, A. Bouzed, Eur. Phys. J. D **23**, 63 (2003)
8. H.-O. Behrens, G.H. Guthöhrlein, B. Hähner, Laser Elektro-Opt. **1**, 27 (1982)
9. G.H. Guthöhrlein, H.P. Keller, Z. Phys. D **17**, 181 (1990)
10. G.R. Harrison, *M.I.T. Wavelength Tables* (The MIT Press, Cambridge, Mass., London, 1969)